JOURNAL OF MATERIALS SCIENCE 30 (1995) 3811–3819

Degassing and surface analysis of gas atomized aluminium alloy powders

S. J. DAVIS, A. P. MIODOWNIK, J. F. WATTS
Department of Materials Science and Engineering, University of Surrey, Guildford, Surrey GU2 5XH, UK

The degassing behaviour and surface characterization of Al–Mg base alloys has been investigated using quadrupole mass spectrometry (QMS) and X-ray photoelectron spectroscopy (XPS). The alloy composition, particle size and the nature of the atomizing gas have been studied in terms of gas evolution and surface composition. XPS has been used both to measure oxide thicknesses and magnesium enrichment ratios. XPS results show that magnesium segregation increases for larger particle sizes and this is supported by QMS, with a correspondingly higher hydrogen evolution on heating being observed for the larger size fractions. High-resolution XPS of the carbon 1s photoelectron peak (C1s) indicates the presence of carbonate component on the as-received magnesium-containing powders. This component is less pronounced on degassed powders indicating the evolution of CO_2 on heating. This observation is supported by thermodynamic calculations.

1. Introduction

Progress in rapid solidification (RS) techniques have led to powder metallurgy (PM) aluminium alloys that possess higher room-temperature strength, fracture toughness, corrosion resistance and improved elevated temperature mechanical properties relative to ingot metallurgy alloys. Such benefits are a result of microstructural refinement, chemical uniformity and extended solid solubility [1]. RS aluminium alloy particles, however, are coated by a hydrated oxide layer which is incorporated into the alloy during subsequent processing. Most PM aluminium alloys have a surface oxide which accounts for less than about 0.6 vol % of the final product. However, problems can arise due to non-uniform distribution of this oxide during processing which leads to a reduction in mechanical properties. This oxide must, therefore, be broken up during consolidation in order to expose fresh metal surfaces and allow bonding between the particles. A better distribution can be achieved by lowering the oxygen level but it is impossible to produce oxide-free powder because oxidation of aluminium is inevitable even under oxygen partial pressures as low as 10^{-54} mbar. It is also possible to reduce the oxygen content by producing larger powders with a low surface to volume ratio; however, such methods reduce the benefits of RS.

Inert gas atomization and handling results in a thin oxide layer, minimizes hydration of the layer, and further reduces the overall oxide content by producing spherical particles. However, the physical state of the atomizing gas (i.e. wet or dry) clearly also affects the level of oxide present on a powder and the associated level of adsorbed and absorbed water. Degassing of powders prior to compaction is, therefore, of great importance and commercial concern. It can eliminate the hydrate from the oxide layer and can strongly influence the effect of the oxide on the final mechanical properties. Inadequate degassing can lead to blistering of the final product and limit the break up of the surface oxide film. This justifies the investigation of the effect of changes in powder production, storage, composition and degassing conditions on the surface morphology, oxide content and segregation of solutes upon heating.

2. The nature of RS powder surfaces

Many researchers, for example Grant and his coworkers, have indicated the problems associated with the consolidation of rapidly solidified powders regarding the role of the oxide layer [2–4]. These researchers highlighted the need to analyse the oxide films on powders and commented that oxide formation was usually poorly monitored and controlled [3]. Froes and Pickens [5] emphasized that the oxide formed on the surface would not dissolve during processing into the base metal and outlined the need for degassing of aluminium alloy powders prior to consolidation. Kim *et al.* [6–8] reported the presence of an amorphous alumina film on a 7091 powder surface and studied the breakup of surface oxides which is affected by the degree of dehydration. When fully dehydrated, the surface oxide film can be completely broken up during subsequent heat treatment. Degassing traces for an Al–Mg alloy showed adsorbed water being liberated at about 100 °C with chemically bonded water and hydrogen liberated at higher temperatures. Hydrogen evolution was associated with a rapid decrease in the water signal and this was

0022–2461

attributed to a chemical reaction with components on the powder surface [7]. Further work on the degassing of 7091 aluminium alloy powders by Ackermann *et al.* [9] again showed a large water peak with a maximum at 200 °C and a peak for hydrogen with a maximum at 400 °C.

Olefjord and Nylund [10] investigated the effects of storage upon the surface state using X-ray photoelectron spectroscopy (XPS) together with sputter depth profiling for an AlMn2.5Cr RS powder. They detected an oxide component by XPS even after ion etching to more than 5 nm below the original surface and proposed an island-like oxide distribution with thick discrete 5 nm regions surrounded by generally thinner 2 nm oxide layers and growth of the hydroxide layer with time and relative humidity.

The effect of varying atomizing gas, temperature and vacuum on the degassing of cold isostatically pressed components has been studied by Schlich *et al.* using quadrupole mass spectrometry (QMS) [11]. It was found that fracture in the non-degassed specimens occurred mainly along prior powder particle boundaries, whereas degassed specimens had an increased strength due to improved powder particle bonding and showed transgranular fracture. Water was desorbed between 120 and 200 °C and hydrogen from 350 °C up to 450 °C. These results are in agreement with the findings of several parallel studies. They also concluded that for complete degassing, the powder should be heated up to the maximum temperature possible (limited by excessive degradation of the structure) and that degassing for a prolonged time at a reduced temperature does not result in complete degassing.

Kirchoff *et al.* [12] looked at ways of improving the degassing cycle to achieve optimum performance for aluminium PM alloys and studied various techniques for measuring the extent of degassing. Density measurements, metallographic evaluation, electrical conductivity and ultrasonic testing all showed some sensitivity to the extremes of degassing conditions. However, techniques such as density measurements, hardness and metallographic evaluation are not suitable for fine tuning of the degassing process and the most reliable method was found to be the use of mass spectrometry to measure the gas evolution from the final product.

Extensive work has previously been carried out at the University of Surrey by various workers [13–15] to investigate the oxide layer and surface segregation in RS aluminium alloy powders. It was reported that magnesium segregation occurred during heat treatment at 425 °C [14]; however, as magnesium was only present in trace amounts in the alloys investigated, it was difficult to validate that result.

Carney has described three different parameters relating to segregation [14]. These are:

(a) a total enrichment factor, E_f^T, which considers segregation of metallic elements in their cationic state through the total analysis depth for XPS;

(b) a surface enrichment factor, E_f^τ, to consider segregation through the oxide; and

(c) an interface enrichment factor, E_f^Φ, which considers segregation in the metal below the oxide.

Magnesium does not exist in its metallic state within the analysis depth for XPS under normal conditions; therefore, it is not possible to determine a value for the interface enrichment factor, E_f^Φ, as this term requires a metallic component to be present. Expressions were developed for segregation in simple binary alloys. Technically when studying a more complicated alloy system, with a greater number of solutes, more complex expressions should be used. However, the equations of Carney *et al.* [13] should be sufficient for obtaining qualitative trends of magnesium segregation, and will thus be used in this study.

Carney *et al.* [13] also derived a method to allow the aluminium oxide thickness to be estimated from a comparison of the metallic and oxidized components of the aluminium 2p XPS spectrum (Equation 1). The following equation enables the oxide thickness, d, to be calculated from a single XPS high-resolution spectrum with only the inelastic mean free path, λ, being required. An empirical value of λ for attenuation of the Al 2p photoelectron in the oxide has been used in this study [16] as any signal from the metallic species is attenuated by the oxide overlayer.

$$d = \frac{\lambda}{2}\ln\left[\frac{I_d^{ox}}{I_d^{me}} + 1\right] \quad (1)$$

3. Experimental procedure

3.1. RS Al alloy powders

Powders used in this study were produced by Metalloys, Birmingham, UK, by high-pressure gas atomization (HPGA) using argon; the series designated "wet" were produced with a low level of water present in the atomizing gas. The dew points were -50 °C and >0 °C for the "dry" and the "wet" atomizing gases, respectively. Powders were sieved to sub 45 μm prior to use in this study; their composition and an explanation of the notation used is given in Table I.

3.2. Degassing apparatus

The degassing equipment is shown schematically in Fig. 1. This consists of a stainless steel ultra-high vacuum (UHV) chamber which is pumped in two stages by a rotary pump and an Edwards EO4 diffusion pump charged with polyphenyl ether (Santovac 5) oil and fitted with a Vacuum Generators CCT liquid nitrogen cold trap (200l min^{-1} pumping speed for nitrogen). A ceramic tube furnace with tungsten heating wires allowed powders to be heated to the desired temperature; the heater was controlled by an R-type (Pt/Pt 13% Rh) thermocouple situated very close to the powder surface to minimize errors in measurement. Quadrupole mass spectrometry (QMS) measurements were made using an Arga residual gas analyser (VG Quadrupoles Ltd) linked to a PC. The quadrupole detector (0–80 Daltons) was situated in the main chamber and allowed the partial pressures of hydrogen, water and carbon dioxide to be recorded as a function of temperature and/or time.

TABLE I Composition of alloys used in this study

Alloy designation	Mg content	Si	Fe	Mn	Mg	Cr	Ni	Mo	W	Al	Comments
A	3% Mg				3.0					Bal.	Binary alloy (nominal composition only)
B	0% Mg	0.02	8.03	0.06	0.01	1.08	0.95	0.9	0.14	Bal.	No magnesium added
C	1% Mg	0.05	7.86	0.06	0.91	0.01	1.0	0.96	0.5	Bal.	Low water ($-H_2O$) 1% Magnesium alloy[a]
D	1% Mg	0.02	7.96	0.06	0.87	0.04	0.5	0.96	0.42	Bal.	High water ($+H_2O$) 1% Magnesium alloy[a]

[a] Water refers to that added to the atomizing gas.

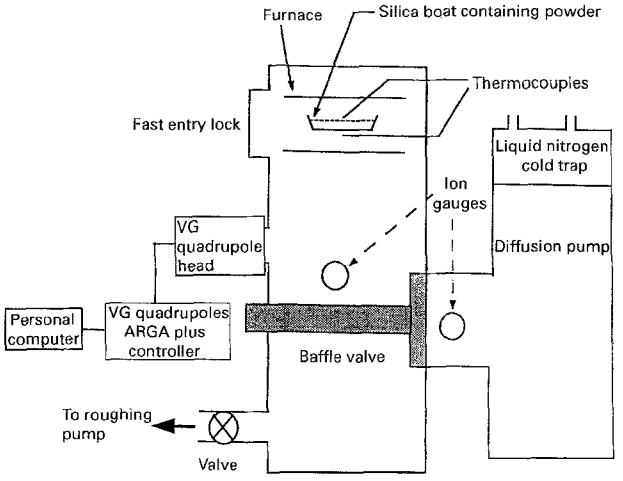

Figure 1 Schematic drawing of the degassing apparatus indicating the position of the quadrupole mass spectrometer.

3.3. Degassing, powder handling and storage

Approximately 5 g powder was placed in a silica boat which was inserted into the tube furnace. To reduce air contact during pumping to ultra-high vacuum (UHV), the chamber was first back-filled with high-purity argon before pumping to a rough vacuum using a rotary pump. At a pressure of about 10^{-2} mbar the diffusion pump was opened to the chamber and the chamber further pumped for about 14 h until a pressure of about 10^{-8} mbar was reached. At all times during analysis the diffusion pump was left open to the chamber to prevent evolved gases from building up in the system. The ion-gauge filament was left running during degassing to enable the total pressure in the system to be monitored.

A heating rate of approximately 3.7 °C min^{-1} was used to heat the powder from ambient temperature to 560 °C in 2.5 h. The cold trap on the diffusion pump was chilled using liquid nitrogen (to give a base pressure of about $< 10^{-8}$ mbar) 15 min before heating to ensure a consistent pumping regime for each experiment.

Prior to heating (but after chilling the trap), a wide scan up to 80 Daltons (80 D) was recorded which gave an indication of the vacuum chamber condition to eliminate the presence of leaks or other anomalies. During the heating process the change in partial pressures of hydrogen (2 D), water (18 D) and carbon dioxide (44 D) were monitored continuously. After ramping to the maximum temperature, this was maintained for 0.5 h and then the chamber was slowly cooled, under UHV, to room temperature. The powder sample was then transferred, under flowing argon inside a glove bag, to specially made glass storage containers and the powders remained in this state until loaded into the photoelectron spectrometer for XPS analysis.

3.4. XPS analysis

Loading the sample into the spectrometer resulted in a brief atmospheric exposure; this was minimized by surrounding the sample with argon whilst the spectrometer was evacuated to UHV. Samples were mounted for XPS analysis using double-sided adhesive tape. This technique has been shown to be acceptable both in terms of vacuum integrity and data acquisition by Carney [14]. It was important that the powder surfaces were presented for analysis in the same condition as they were produced and this prevents the use of green compacts.

A VG Scientific ESCA 3 MkII interfaced to VG 3040 data system based on a DEC PDP8e computer was used in this study. AlK_α radiation (1486.6 eV) was used (300 W anode power) with a nominal 45° take off angle (relative to the plane of the specimen holder). As the spherical nature of the powders makes the take off angle non-critical, an angle of 45° was used to provide maximum sensitivity. Spectra were acquired in the constant analyser energy (CAE) mode at a pass energy of 50 eV. Chemical quantification was achieved by removing a linear background from the high-resolution spectrum of the element concerned and calculating the intensity (area) of the peak. Peak areas were then normalized using appropriate sensitivity factors [17]. A more sophisticated routine was adopted to peak fit the aluminium 2p signal [18]. A linear background was fitted to the Al 2p peaks and the metallic and oxide components were resolved using an iterative least squares fitting routine.

3.5. Presentation of degassing results

After testing various methods of presenting the results it was decided to use plots of partial pressure of the

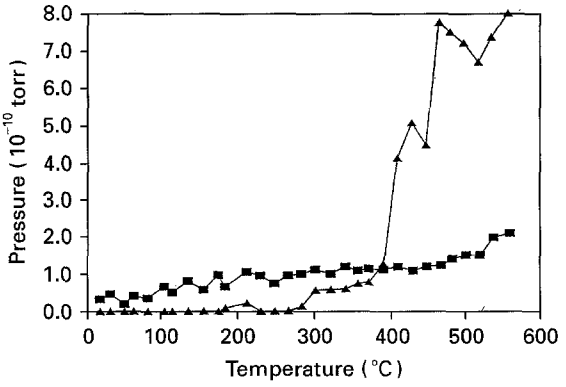

Figure 2 Hydrogen evolution from (▲) a 3% Mg powder alloy (A) compared to (■) a blank chamber.

evolved species versus temperature. It was not deemed necessary to remove a background trace from the degassing results obtained as this made very little difference due to the signal from a blank chamber being significantly lower than that for a chamber containing powder, Fig. 2. This was expected as only a small region of the chamber was heated to sufficient temperatures to promote degassing.

4. Degassing results

4.1. Effect of pumping time

Increasing exposure to UHV from 12–72 h showed a significant reduction in the evolution of water, due to physically bonded water being removed by the continuously pumped UHV chamber. It was therefore important to keep the time spent under UHV prior to analysis constant, and an overnight pumpdown (12 h) was used.

4.2. Effect of magnesium content

The evolution of water, hydrogen and carbon dioxide as a function of temperature for alloys with varying magnesium content is shown in Fig. 3. For alloys containing magnesium there was considerable hydrogen evolution above about 400 °C which coincided with a sharp decrease in the water peak. This is consistent with the suggestion by previous workers that the evolved water reacts with magnesium on the powder surface causing hydrogen to be liberated

$$Mg_{(s)} + H_2O_{(l)} = MgO_{(s)} + H_{2(g)}\uparrow \quad (2)$$

There was no sharp decrease in the water peak for magnesium-free alloys, which gives further confirmation that water is only consumed when involved in a reaction with magnesium. Plotting the evolution of water (Fig. 4a) and hydrogen (Fig. 4b) for alloys with different magnesium contents enables this effect to be seen more clearly. As the magnesium content is increased, the alloys also show a progressive reduction in the evolution of water at lower temperatures (100–180 °C), consistent with increasing chemisorption of the water rather than the presence of physically absorbed layers.

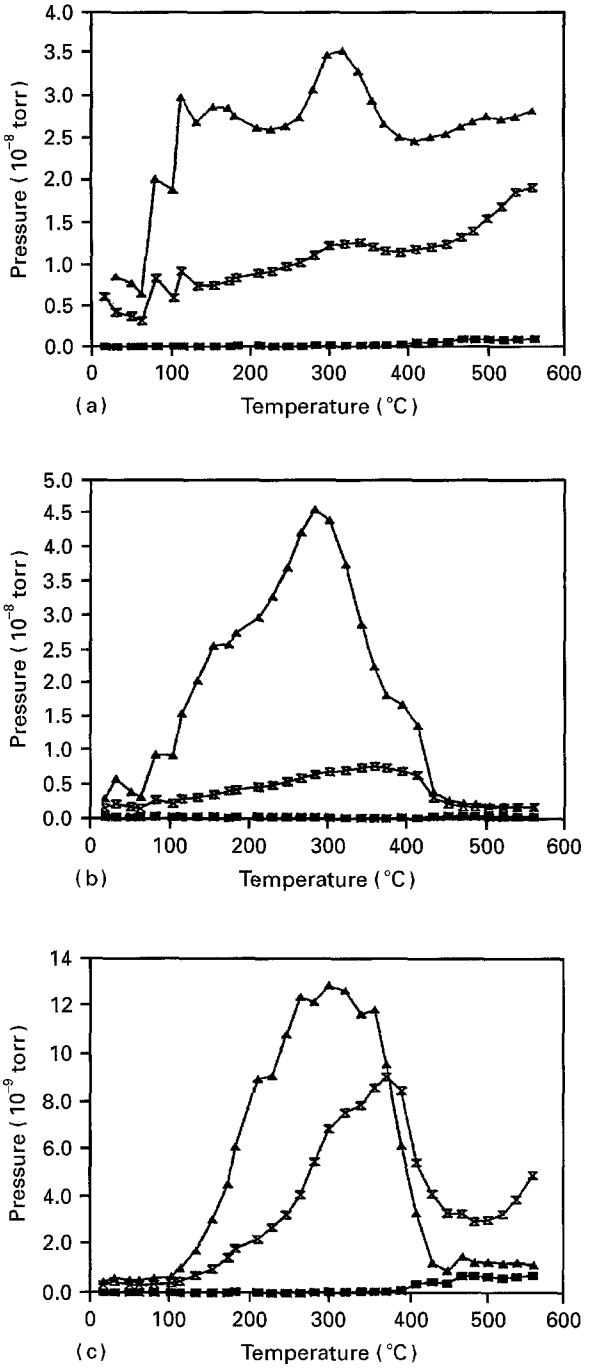

Figure 3 Evolution of (■) hydrogen, (▲) water and (⊠) carbon dioxide from a series of powders with varying magnesium concentrations: (a) 0% Mg alloy (B), (b) 1% Mg alloy (C), (c) 3% Mg alloy (A).

4.3. Effect of water in the atomizing gas

The 1% Mg alloy has been produced using both dry and wet atomizing gases (Alloys C and D). The results from these experiments are rather similar, with slightly more evolution from the powder atomized with dry gas (Fig. 5a). It is not surprising that only a small difference was observed, as water introduced during atomization is likely to be chemisorbed and thus will not evolve until higher temperatures. At such temperatures, evolution is associated with the back reaction of water with magnesium and it is therefore more useful to study the evolution of hydrogen which increases from about 400 °C (Fig. 5b). The results are

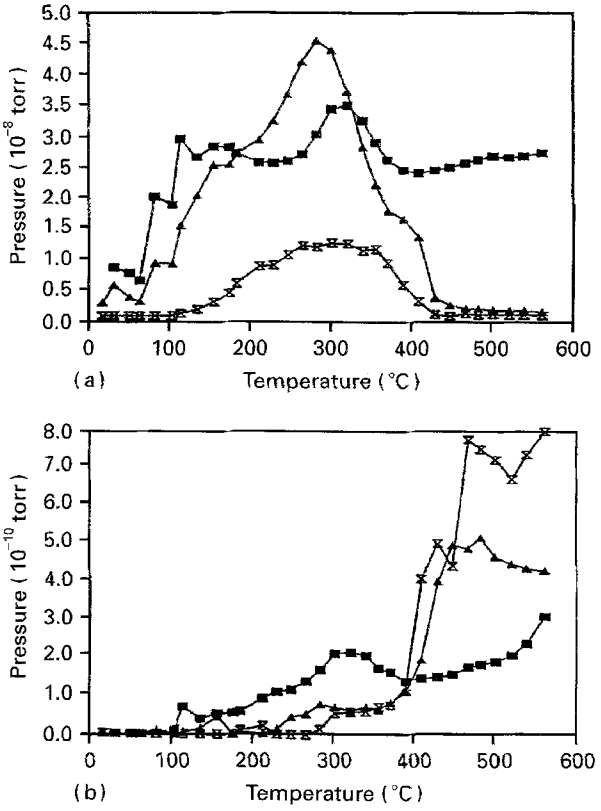

Figure 4 Comparative plots showing (a) water evolution, and (b) hydrogen evolution, from powders with differing magnesium concentrations: (■) 0%, alloy B; (▲) 1%, alloy C, (⧖) 3%, alloy A.

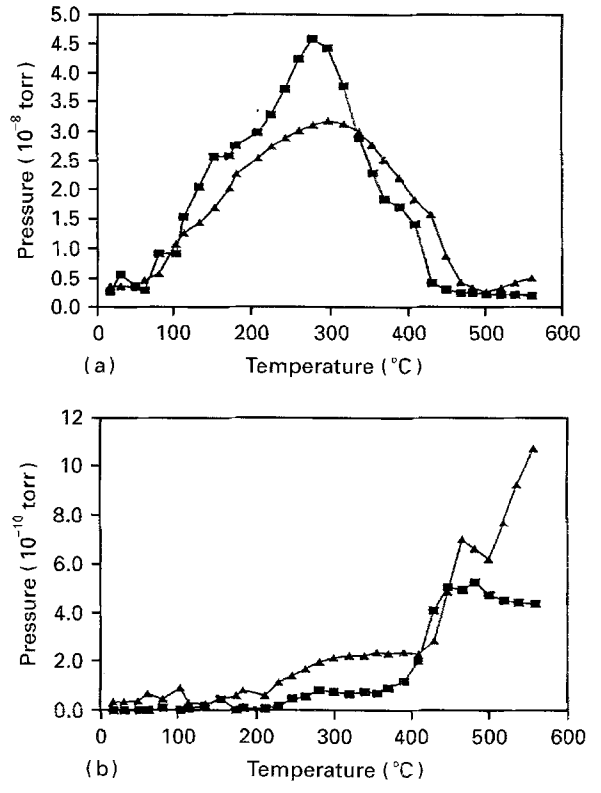

Figure 5 (a) Water evolution, and (b) hydrogen evolution, from powders produced (▲) with and (■) without water in the atomizing gas.

consistent with there being more chemisorbed water present on powders produced with "wet" atomizing gas. It is this water which is subsequently evolved at the higher temperatures and which reacts with the

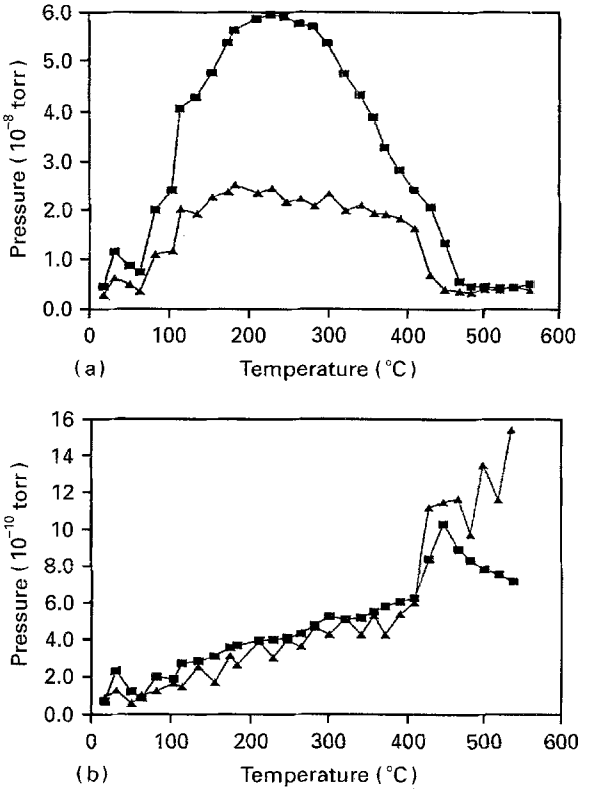

Figure 6 (a) Water evolution, and (b) hydrogen evolution, from a 1% Mg powder sieved to different size fractions: (■) 1–5 μm, (▲) 30–50 μm.

magnesium present to form hydrogen. Powders produced under dry conditions may have a higher peak evolution of water at low temperatures but at the higher temperatures where back reaction is likely, they actually evolve less water. Hence the hydrogen peak for such alloys shows a plateau at about 400 °C, instead of continually increasing as in the case of the wet atomized powders.

4.4. Effect of particle size

Degassing was carried out on the two extreme size fractions (1–5 μm and 30–50 μm) and results obtained for both water and hydrogen evolution are given in Fig. 6.

Water evolution is greatest from the small size fraction; this is to be expected as the smaller powder particles will have a higher specific surface area. However, if gas evolution increased proportionately to the powder surface area, evolution from the smaller size fraction should be orders of magnitude greater than for the larger size fraction. In practice, the difference is only a factor of two higher. This anomaly is probably due to the degree of gas entrapment caused by powder settling in the powder holder on heating.

The degassing characteristics of the various powder size fractions proved interesting; water evolution was greatest for the small size fractions and this was expected as these powders have a much higher surface area for desorption. The hydrogen evolution, however, followed the opposite trend with an increased high-temperature evolution occurring for the large size fractions. XPS of the powders showed higher

TABLE II Enrichment factors for P3.3.0 alloy as a function of powder size fraction

Alloy	E_f^T	E_f^x
1% Mg (4–12 μm) (C)	6.89	8.91
1% Mg (12–18 μm) (C)	12.69	15.50
1% Mg (Av = 25 μm) (C)	12.12	13.01
1% Mg (30–50 μm) (C)	18.71	21.34

magnesium segregation for the large particles (Table II), this was expected as during atomization these particles remain energetic for longer thus allowing more segregation to occur [13]. This results in a powder with an increased surface magnesium concentration and as before leads to an increased hydrogen signal from the magnesium-rich surface. The direct evidence via XPS for increased magnesium segregation in the large-size fractions is therefore also confirmed by the indirect measurements of surface reactions made by quadrupole mass spectrometry.

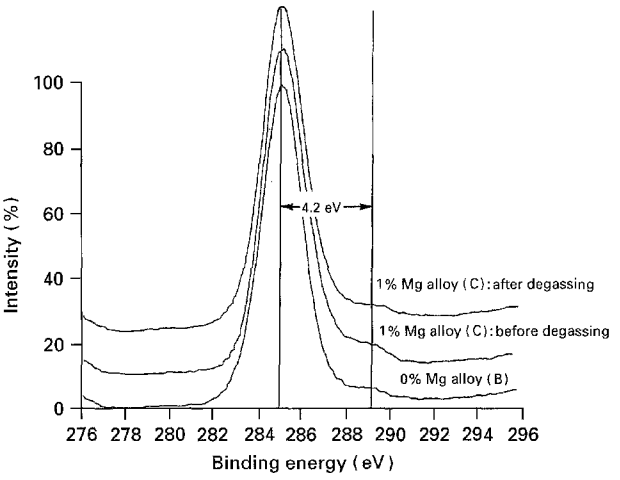

Figure 8 XPS high-resolution C 1s spectra showing a component at a 4.2 eV shift for the magnesium-containing powders.

5. XPS results

A typical XPS survey spectrum for an Al 1% Mg base alloy powder is given in Fig. 7. Peaks from silicon and chlorine can be assigned to the mounting medium. Examination of the high-resolution carbon 1s (C 1s) region for the magnesium-containing alloy (Fig. 8) shows a shoulder on the high binding energy side at a shift of 4.2 eV. This is not present for the 0% Mg alloy (B) and decreases when the Al 1% Mg alloy (C) has been degassed. It is suggested that $MgCO_3$ is present as a surface layer on the as-received magnesium-containing powders as this forms readily ($\Delta G_{formation} = -1030\,kJ\,mol^{-1}$ at 300 K [19]).

5.1. Enrichment ratios

Values of enrichment factors have been calculated for magnesium in aluminium and values of E_f^T and E_f^x are reported in Table III. Degassing does not appear to effect the enrichment of magnesium in aluminium for these powders. This is to be expected as the degassing temperatures are much lower than the melting point. The values obtained are in agreement with those previously calculated by Carney *et al.* [13]. The results

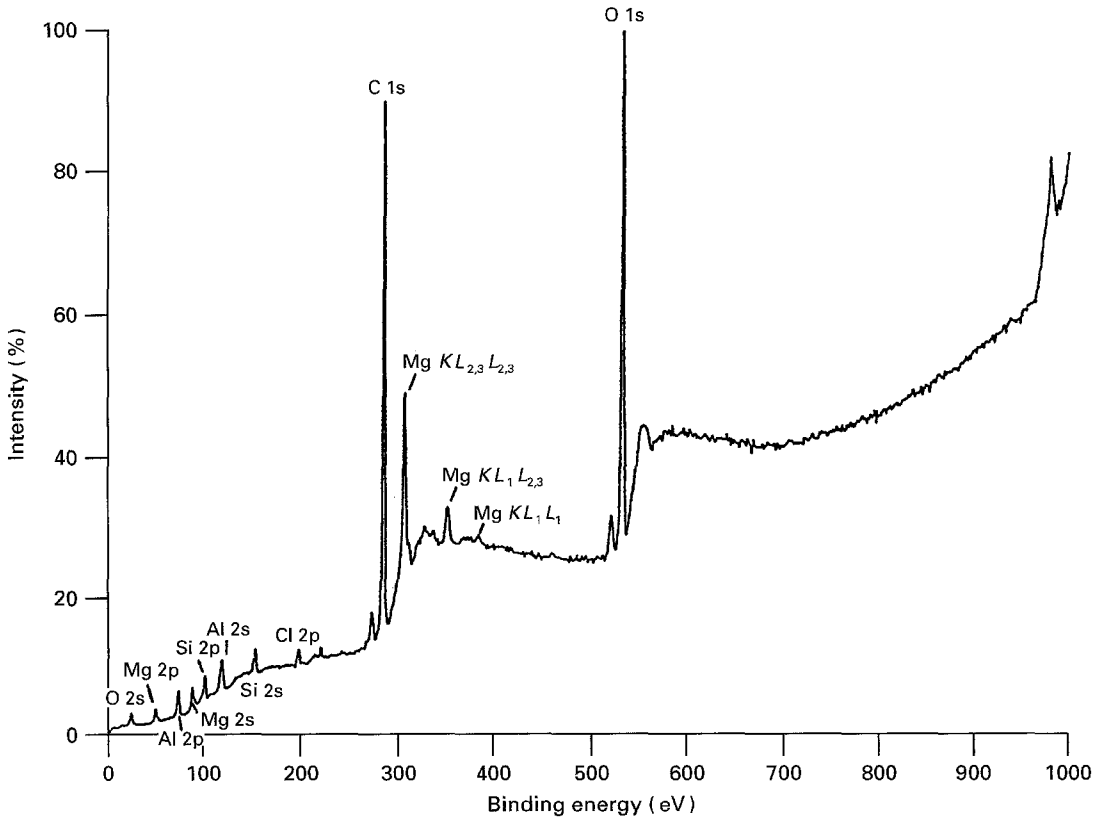

Figure 7 XPS survey spectrum for a 1% Mg powder (Alloy C).

TABLE III Total E_f^T, and sufrace E_f^s, enrichment factors for certain size fractions of the alloys studied

Alloy composition	Alloy designation	Size fraction (μm)	E_f^T		E_f^s	
			As received	Degassed	As received	Degassed
3% Mg°	(A)	< 45	n.d.	3.17	n.d.	3.83
1% Mg°	(D)	< 45	6.86	9.34	7.88	10.77
1% Mg°	(C)	< 45	12.12	9.14	13.01	11.09
0% Mg°	(B)	< 45	[a]	[a]	[a]	[a]
1% Mg°	(C)	1–5	9.50	7.01	11.71	8.70
1% Mg°	(C)	30–50	7.75	2.44	9.31	2.94
1% Mg#	(C)	1–5	13.77	n.d.[b]	17.62	n.d.[b]
1% Mg#	(C)	4–12	6.89	n.d.[b]	8.91	n.d.[b]
1% Mg#	(C)	12–18	12.69	n.d.[b]	15.50	n.d.[b]
1% Mg#	(C)	30–50	18.71	n.d.[b]	21.,34	n.d.[b]

[a] Mg in trace quantities only.
[b] n.d. not determined.
° Powders stored before analysis.
XPS performed on freshly received powders stored in glass jars.

for particles in the 4–50 μm range confirm enhanced magnesium segregation for larger size fractions (Table II). However, the results for < 5 μm particles do not fit this trend possibly due to high carbonaceous contamination on this smallest size fraction.

It is also interesting to compare the values obtained for the 1% Mg alloy (Alloy C) which has merely been sieved to < 45 μm. The mean diameter corresponds to about 25 μm and the values of enrichment factors calculated for this alloy are in keeping with values obtained for a similar size fraction in the screened powders.

There is a discrepancy when comparing the enrichment ratios for both small and large size fractions for the as-received powders and stored powders, which can be attributed to increased carbon contamination on the surface of the stored powders (Table IV). The stored powder had a higher percentage of carbon on the oxide surface leading to attenuation of the aluminium and magnesium signals. There is a large difference between the binding energies of the Al 2p(75 eV) and the Mg 1s (1305 eV) resulting in associated differences in their inelastic mean free paths (Mg 1s ≪ Al 2p). The signal given by the Mg 1s is therefore affected to a greater extent than the Al 2p and thus less magnesium is detected. It is theoretically possible to take into account the attenuating carbonaceous overlayer by using an appropriate modification of the Beer–Lambert equation; however, the spherical nature of the particles makes this an uncertain process and for this reason we merely note the effect.

TABLE IV Effect of adventitious carbon on the calculated total enrichment factors

Alloy	As-received		Stored	
	E_f^T	Carbon (at %)	E_f^T	Carbon (at %)
1% Mg (30–50 μm) (C)	18.71	39.0	7.75	73.4

TABLE V Oxide thicknesses determined by XPS

Powder description	Alloy designation	Oxide thickness (nm)	
		As-received	De-gassed
3% Mg	A	–	1.98
1% Mg "wet"	D	2.42	2.33
1% Mg "dry"	C	(3.06)[b]	1.97
0% Mg	B	2.38	2.17
1% Mg (1–5 μm)	C	1.85	1.88
1% Mg (30–50 μm)	C	2.03	2.14
1% Mg (1–5 μm)	C[a]	1.56	–
1% Mg (4–12 μm)	C[a]	1.68	–
1% Mg (12–18 μm)	C[a]	1.81	–
1% Mg (30–50 μm)	C[a]	2.14	–

[a] XPS performed on freshly received powders stored in glass jars.
[b] denotes a poor peak fit due to an abnormally high inelastic background.

5.2. Oxide thicknesses

Using Equation 1 above and the accepted EFC value of 2.48 nm (Olefjord *et al.* [16]), oxide thicknesses were calculated for both the as-received and the degassed powders and the results are summarized in Table V. Degassing does not appear to affect the aluminium oxide thickness. This result is not unexpected, as degradation of the oxide is unlikely at these temperatures. It is important to distinguish between the total oxide thickness and the aluminium oxide thickness estimated using this XPS measurement technique; fitting the Al 2p spectra only allows the aluminium component of the oxide to be calculated. Owing to magnesium segregation it is, however, likely that there is also a magnesium oxide component present on the surface and this leads to the suggestion of a layered oxide structure. Ideally the total oxide thickness should be measured, as it is this value which will affect the amount of oxide inclusion in the final component. Oxide thicknesses for the different size fractions increase with increasing particle size which might be expected as larger particles remain hotter for longer during atomization. It is also interesting that the oxide thicknesses are below the suggested Mott thickness of 2 nm, in agreement with the findings of Carney *et al.* [13].

6. Correlation of surface analysis with thermodynamics

The aluminium oxide thickness has been calculated using a self-consistent XPS technique and results indicate that the oxide is very thin (~ 2 nm), less than the Mott thickness and consistent with work of Carney [14]. This is significantly lower than the thickness reported by Olefjord and Nylund [10] where thick islands (5 nm) surrounded by a 2 nm thick oxide layer were suggested. XPS analysis of powders before and after degassing allowed any compositional changes to be determined and results indicated that the oxide thickness did not change upon heating in UHV up to 560 °C. This was not unexpected as aluminium oxide cannot be reduced at these temperatures due to the large change in free energy of formation ($\Delta G_f = -1560$ kJ mol^{-1} at 300 K and -1345 kJ mol^{-1} at 1000 K for γ Al_2O_3 [19]. The oxide thickness measurement by XPS, however, only refers to the aluminium oxide thickness and does not consider oxides from other alloying elements such as magnesium. Other surface species such as carbonates are also likely to play a role in the surface reactions. Close inspection of the C 1s high-resolution spectra for magnesium-containing alloys shows a broadening on the high BE side of the peak. This is attributed to a component at a 4.2 eV shift which is typical of a carbonate. The XPS of the 0% Mg alloy (B) does not show this feature. Furthermore, on degassing, this component decreases, consistent with the breakdown of carbonate species present on the surface. It is likely that the decomposition of magnesium carbonate: $MgCO_{3(s)} \rightarrow MgO_{(s)} + CO_{2(g)}$ occurs on heating and this is supported by thermodynamic calculations where the stability of different species is considered as a function of temperature and pressure. Fig. 9 shows the relevant Ellingham diagram calculated for the above reaction, where the van't Hoff Isotherm has been utilized to correct for pressure. It is clear that $MgCO_3$ becomes unstable on heating.

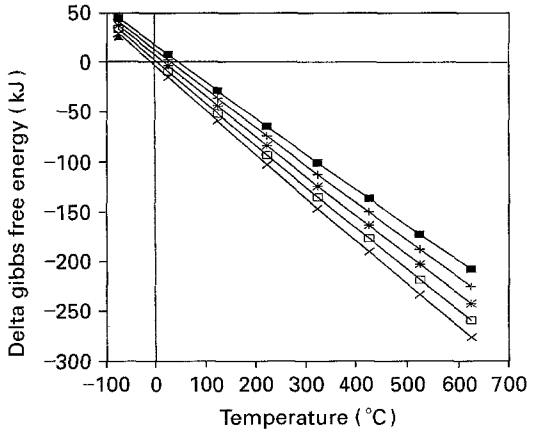

Figure 9 Free energy/temperature diagram for the decomposition of $MgCO_{3(s)} \rightarrow MgO_{(s)} + CO_{2(g)}$ corrected for pressure using the van't Hoff Isotherm. CO_2 partial pressure: (■) 1×10^{-7} torr, (+) 1×10^{-8} torr, (*) 1×10^{-9} torr, (□) 1×10^{-10} torr, (×) 1×10^{-11} torr.

7. Conclusions

1. Quadrupole mass spectrometry in conjunction with powder heating in UHV provides an excellent method to study surface reactions with the combination of surface analysis and degassing allowing a more complete picture of the surface chemistry involved to be obtained.

2. The high-temperature hydrogen evolution (400 °C) is a product of back-reacted chemisorbed water with surface enriched magnesium

$$Mg_{(s)} + H_2O_{(l)} > MgO_{(s)} + H_{2(g)}\uparrow$$

and is dependent upon the level of chemisorbed water and increases with the concentration of magnesium present at the surface.

3. Enrichment ratios for magnesium in aluminium have been determined by XPS; there is an increase in enrichment with particle size. This is confirmed by an increased hydrogen evolution above about 400 °C for the larger size fractions.

4. The aluminium oxide thickness appears fairly constant at about 2 nm and is not changed on degassing in UHV up to about 560 °C. The oxide thickness, however, does increase with increasing particle size and this is consistent with the larger fraction remaining hot for longer and therefore undergoes increased oxidation.

5. Magnesium carbonate exists on the powder surface; evidence for a breakdown on degassing has been provided by analysis of the high resolution C 1s spectra and also from thermodynamic calculations.

Acknowledgements

One of the authors (S.J.D.) gratefully acknowledges partial support from EURAM Grant MA1E/0076/C, and P. Smith, Alpoco Ltd, for the supply of the powders under that contract. We also thank Dr T. J. Carney and Dr P. Tsakiropoulos for invaluable discussions.

References

1. H. JONES, *Philos. Mag.* **B61** (1990) 587.
2. N. J. GRANT, *J. Metals* **35** (1983) 20.
3. *Idem*, in "Conference on Rapidly Solidified Powders", Wurzburg, 1984, edited by S. STEEB and H. WARRLIMONT (1984) p. 3.
4. *Idem*, in "Advances in Powder Technology" (1980) Ch. 1, p. 1.
5. F. H. FROES and J. R. PICKENS, *J. Metals* **36** (1984) 14.
6. Y. W. KIM, W. M. GRIFFITH and F. H. FROES, ASM Metals/Material Tech Series No 8305-048 (1984).
7. *Idem*, *J. Metals* **37** (8) (1985) 27.
8. *Idem*, "Rapidly solidified powder Al alloys", ASTM STP 890, edited by M. E. FINE and E. A. STARKE Jr (ASTM, Philadelphia, PA, 1986) p. 283.
9. L. ACKERMANN, I. GUILLEMIN, R. LALAUZE and C. PIJOLAT, in "High Strength PM Al alloys 2", edited by G. J. HILDERMAND and M. J. KOCZAK (Metallurgical Society of AIME, Warrendale, PA, 1986) p. 175.
10. I. OLEFJORD and A. NYLUND, *Surf. Interface Anal.* **12** (1988) 401.
11. H. SCHLICH, M. THUMANN and G. WIRTH, "PM Aerospace Materials", paper 31 (1987).
12. S. D. KIRCHOFF, J. Y. ADKINS, W. M. GRIFFITH and I. A. MARTORELL, "Rapidly Solidified Powder Aluminium Alloys", ASTM STP 890, edited by M. E. FINE and E. A. STARKE Jr (ASTM, Philadelphia, PA, 1986) p. 354.

13. T. J. CARNEY, P. TSAKIROPOULOS, J. F. WATTS and J. E. CASTLE, *Int. J. Rapid Solid.* **5** (1990).
14. T. J. CARNEY, PhD thesis, University of Surrey, Guildford (1990).
15. J. F. WATTS and T. J. CARNEY, in "Powder Metallurgy: An Overview", edited by J. V. Wood (The Institute of Metals, London, 1991) pp. 76–99.
16. I. OLEFJORD, H. J. MATHIEU and P. MARCUS, *Surf. Interface Anal.* **15** (1990) 681.
17. D. BRIGGS and M. P. SEAH, in "Practical Surface Analysis", 2nd Edn (Wiley, Chichester, 1983) Appendix 6.
18. P. M. A. SHERWOOD, *ibid.*, Appendix 3.
19. D. R. STULL and H. PROPHET, Project Directors, "JANAF Thermochemical Tables", 2nd Edn (Office of Standard Reference Data, National Bureau of Standards, Washington, DC, 1970).

Received 16 September 1994
and accepted 3 February 1995